Article

pubs.acs.org/Biomac

Micro/Nanostructured Hyaluronic Acid Matrices with Tuned Swelling and Drug Release Properties

Yanina Minaberry,[†] Diego A. Chiappetta,[‡,§] Alejandro Sosnik,[‡,§] and Matías Jobbágy*[,†,§,∥]

[†]INQUIMAE-DQIAQF, Facultad de Ciencias Exactas y Naturales, Universidad de Buenos Aires, Ciudad Universitaria, Pab. II, C1428EHA, Buenos Aires, Argentina

[‡]The Group of Biomaterials and Nanotechnology for Improved Medicines (BIONIMED), Department of Pharmaceutical Technology, Faculty of Pharmacy and Biochemistry, University of Buenos Aires, Buenos Aires, Argentina.

[§]National Science Research Council (CONICET)

[∥]Centro Interdisciplinario de Nanociencia y Nanotecnología

S *Supporting Information*

ABSTRACT: Hyaluronic acid (HA) hydrogels were structured in the form of porous monoliths by means of the ice-segregation-induced self-assembly (ISISA) method coupled with freeze−drying. Physical and chemical parameters were explored in order to fine-tune the microstructure and the incidence on both swelling and dissolution behavior in aqueous media. Gentamicin-loaded HA matrices with tuned drug release properties were also prepared; their inherent properties and behavior in solution are discussed in the framework of thermal analysis and scanning electron microscopy inspection.

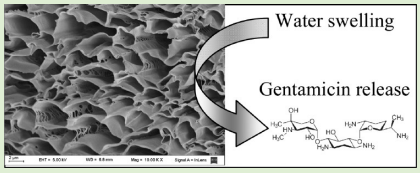

1. INTRODUCTION

Tissue engineering triggered the development of hydrogels made of biocompatible and biodegradable biopolymers that mimic the extracellular matrix (ECM).[1] These matrices could serve as scaffolds enhancing regeneration because cells are induced to self-assemble into a 3D tissue-like structure. These hydrogels are also expected to display additional key roles, including the sustained release of drugs and/or growth factors, responsiveness to environmental stimuli, and so forth. In this sense, much effort is currently being devoted to improve and expand the performance and the application of well-accepted biopolymers by means of the rational and controlled structure formation in the form of scaffolds exhibiting sophisticated 3D architectures. Textural properties, in particular, micro- and macroporosity, are expected to be fine-tuned to generate a well-interconnected porous network that not only allows efficient cell attachment, migration, and proliferation, but also favors a proper mass transport and exchange of nutrients and waste products.[2−5]

Among the biopolymers employed in this field, hyaluronic acid (HA), a linear polysaccharide consisting of alternating units of a repeating disaccharide, β-1,4-D-glucuronic acid-β-1,3-*N*-acetyl-D-glucosamine (see Figure S1), has gained much attention due to its proven cyto- and biocompatibility and biodegradability.[6−8] However, the structure formation of inherently chemically and thermally labile macromolecules such as HA restricts the number of strategies that can be pursued. The structuring agents should be biocompatible or easily removable, and their use should enable the loading of different active compounds such as drugs and growth factors. Previous studies reported on the effectiveness of structured HA/collagen scaffolds for skin repair, in particular, when these systems were loaded with antibiotics that prevented associated wound infections.[9] However, the degree of stucture formation achieved was low and the performance of the drug delivery systems relatively poor.[10−12] Thus, this scenario claims alternative structure formation methods that lead to scaffolds with improved features.

The ice-segregation-induced self-assembly (ISISA) method was demonstrated to be an outstanding tool for the construction of sophisticated monoliths or fibers, with exquisite control of pore size, shape, distribution, orientation, and interconnectivity.[13] The versatility offered by ISISA lies in the possibility of tuning the textural properties of the monolith with several physicochemical parameters, such as solvent composition, solute nature and concentration, freezing rate, and temperature gradient, among others. The process involves the exposure of an aqueous gel, solution, or suspension to freezing temperatures. The controlled ice formation, typically in the hexagonal lattice, drives the segregation of every solute or colloid originally dispersed in the aqueous phase toward the zones in which the ice is absent, giving rise to a hierarchical assembly defined by walls, fibers, or bicontinuous arrays of matter surrounding empty areas where the ice resided before sublimation.[13,14] This controlled structure formation process results in a well-organized 3D porous monolith. Owing to the ability to texture large pieces, in the range of centimeters, with pores aligned in a preferential direction, ISISA entails a

Received: May 24, 2012
Revised: November 12, 2012
Published: November 19, 2012

dx.doi.org/10.1021/bm300814h | *Biomacromolecules* 2013, 14, 1−9

promissory future in the field of biomaterials science, tissue engineering, and drug delivery.[15,16] From a chemical point of view, diverse monoliths or scaffolds ranging from strictly ceramic phases to living-cell loaded polymers can be obtained by this process.[17−22] Very recently, it has been reported that bare HA submitted to ISISA spontaneously assembles into 3-D scaffolds that preserve the swelling properties of their chemically cross-linked counterparts and remain stable to dissolution in the scale of hours.[23] The aim of the present work was to demonstrate the potential of the ISISA texturing method for the production of gentamicin (see Figure S2) (G)-loaded HA scaffolds with tunable texture and release properties. The effect of the main preparative variables on the final texture as well as their incidence in the hydration and G release ability were comprehensibly explored.

EXPERIMENTAL SECTION

Sample Preparation. Sodium hyaluronate (HA, $M_w = 2 \times 10^6$ Da, Genzyme) aqueous solutions were prepared in deionized water. Concentrations ranged between 0.1% and 5% weight/volume. Samples were denoted H-X where X represents the weight percentage of HA in solution. To assess the effect of hydrolysis on the properties of the structured matrix, HA (2.5 g) was dissolved at room temperature under vigorous stirring in 100 mL of different sodium phosphate buffer solutions (PBS, pH values of 2, 7, and 12). Buffers presented a final ionic strength of 0.15. The influence of temperature on the HA chemical stability was also evaluated; the aforementioned solutions with fixed pH were incubated without stirring in a thermostated water bath (at 60 °C) for 24 h and denoted with the suffix T. Then, each sample was cooled to room temperature, frozen, and lyophilized. For the preparation of drug-loaded HA scaffolds, gentamicin sulfate (final concentration 20 mg/mL of HA solution, 2%) was dissolved in 1 and 2.5 wt % HA solutions and the preparation procedure repeated as described above; these samples are denoted as H-1.0-G and H-2.5-G, respectively.

Structure Formation by ISISA. HA solutions were poured in molds, typically 1 mL insulin syringes (length 80 mm, diameter 4 mm), and unidirectionally frozen by dipping the mold at a defined rate into a liquid nitrogen (−196 °C) cold bath. Unidirectionally frozen samples were freeze−dried using an Alpha 1−2 LD Plus freeze−dryer. The monoliths were stored at room temperature in a desiccator for further characterization.

Morphological Characterization. The microstructure of the scaffolds obtained under different conditions was characterized by scanning electron microscopy (FESEM Zeiss Supra-40). Pore size and wall thickness of the monoliths were determined from FESEM micrographs of cross sections obtained in the freezing direction. For each construct, at least 20 measurements of pore width and wall thickness were made on each micrograph. Results are expressed as mean value ± SD.

Preparation of HA Samples for MALDI-TOF Mass Spectrometry. Samples (1 wt % HA concentration) prepared as described previously for studies of hydrolysis and thermal degradation were used for MALDI-TOF analysis. MALDI-TOF spectra were acquired on a Bruker Autoflex mass spectrometer (Bruker Daltonics). The system utilizes a pulsed nitrogen laser, emitting at 337 nm. The extraction voltage was 20 kV. For all spectra, 128 scans were acquired using a linear mode, negative and positive. The laser strength was kept about 5% over the threshold setting to achieve the best signal-to-noise ratio. For all samples, a 10 mg/mL 2,5-dihydroxybenzonic acid (DHB) solution in water containing 0.1% trifluoroacetic acid was used as matrix. All HA samples were mixed with the matrix prior to their deposition onto MALDI target 1:10 (V/V). One drop (0.1 μL) of this preparation was placed onto a MALDI-sample plate and afterward dried rapidly under a moderate warm air stream. Spectra were processed with *Flex Analysis* software.

Differential Scanning Calorimetry (DSC). The thermal stability of the HA scaffolds was analyzed by DSC (Mettler Toledo TA-400 differential scanning calorimeter). Samples (3−5 mg) were sealed in 40 μL Al-crucible pans and heated from 25 to 300 °C at 10 °C/min under nitrogen atmosphere. All samples were run in duplicate.

Powder X-ray Diffraction (PXRD). Bare HA, G, as well as G-loaded monoliths were characterized with a Siemens D5000 PXRD equipment using graphite-filtered Cu K_α radiation (λ = 1.5406 Å) between $5° < 2\theta < 70°$, 0.02° scan steps and 1 s integration time.

Swelling. The swelling of the different scaffolds was studied in phosphate buffered solution (PBS, pH 7.4), at 37 °C. Scaffolds were accurately weighed (W_0) and immersed in preheated PBS. At predetermined time intervals, the swollen scaffolds were wiped off with soft tissue paper and weighed (W_t); the degree of swelling for each sample at time t was calculated by using the expression $(W_t - W_0)/W_0 \times 100$.

In Vitro Drug Release/Permeation. Cellulose nitrate membranes (0.45 μm) (Sartorius Stedim Biotech GmbH) were mounted in homemade polypropylene vertical diffusion cells and maintained at 37 °C in a heated compartment. The cell includes a donor chamber (volume = 0.2 mL) and a receiver chamber (volume = 1.6 mL) which was filled with preheated PBS (pH 7.4) (see Figure S3). This setup ensured sink conditions over the whole release assay. These conditions aim to maintain the drug concentration in the release medium ten times smaller than the drug saturation limit that is the intrinsic solubility of the drug in the same medium, namely, approximately 50 mg/mL. After verifying the absence of leakages in the receiver chamber, G-loaded HA scaffolds were immersed in the donor chamber and the drug concentration in the receiver chamber monitored over 8 h. To quantify the total permeated drug, aliquots were collected at predetermined time intervals and assayed by capillary electrophoresis (see below).

Capillary Electrophoresis (CE). CE separations were performed with a P/ACE MDQ Capillary electrophoresis system (Beckman), equipped with diode array detector (190−600 nm), and data processed by *Karat* v 8 software. An uncoated fused-silica capillary of 50 cm length (40 cm to detector) and 75 μm i.d. (MicroSolv Technology) was employed. The separation was carried out using a 150 mM borate buffer at pH 9.4 and a positive voltage of 10 kV with pressure (0.1 psi). Samples were introduced into the capillary by pressure at 0.5 psi for 5 s. UV detection was set at 195 nm and a temperature of 25 °C was employed.

RESULTS AND DISCUSSION

Texturing of HA Scaffolds. The present study was focused on the preparation of HA scaffolds from aqueous solutions with the eventual addition of gentamicin (G) or sodium phosphate buffers, in order to evaluate the role of pH on the structure formation process. The thermal gradient was established between ambient (298 K) and liquid N_2. Despite the structuring process following several common trends, ruled by the physics of phase segregation and irrespective of the nature of the solid, some peculiar fingerprints at the molecular or the nanoscale level can affect the final structure, imposing a careful experimental screening for each new system under investigation.[14]

As a starting point, a family of bare HA scaffolds was prepared by means of increasing the HA concentration and/or the freezing rate; Figure 1 (upper row) presents the texture observed for a series of monoliths prepared under representative conditions. All the samples maintained both the shape and the size of the parent container, in which the parent gel was confined prior to ISISA. Since the ice-front progress state reached a stationary value (e.g., nominal) especially at the upper half of the monolith, characterizations were always conducted on that portion.[24] SEM inspection of their transverse section revealed a homogeneous texture, the pore pattern being only slightly altered in a small region a few hundred micrometers away from the external surface and

dx.doi.org/10.1021/bm300814h | *Biomacromolecules* 2013, 14, 1−9

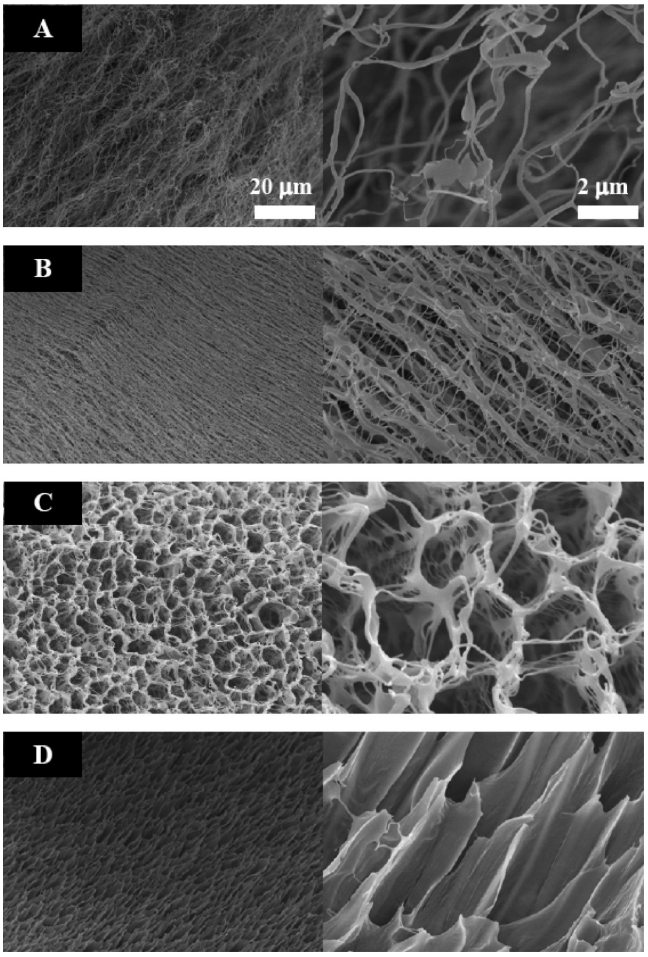

Figure 1. FESEM micrographs (perpendicular to the freezing direction) of HA hydrogels submitted to ISISA with different freezing rate (FR): H-0.1, FR = 3.6 mm min^{-1} (A), H-0.5, FR = 48 mm min^{-1} (B), H-1.0, FR = 1.8 mm min^{-1} (C), and H-2.5, FR = 48 mm min^{-1} (D). Scale bars depicted for sample A are valid for all the images belonging to the same row.

parallel to the freezing direction. This is an experimental feature of this method.[25] Figure 1 shows images of transverse sections of monoliths mounted as a whole; the pores are randomly oriented, exhibiting dimensions of around 10 μm. Representative FESEM images of the HA scaffolds illustrate the different textures achieved by increasing the concentration of native HA in the aqueous solution, ranging from 0.1 to 5 wt %, under gradually faster freezing rates (1.8, 3.6, and 48 mm min^{-1}).

For low HA contents (0.1 and 0.5 wt %), FESEM images showed a fiber-like appearance without any preferential orientation. However, for the lower freezing rate, secondary large pores were apparent, suggesting the templating effect of large ice crystals (see Figure S4). Sample H-0.5 denoted the presence of thicker main fibers laterally bridged by thinner ones, giving rise to a true 3D interconnected network (Figure S5). Once the concentration increased to 1 wt %, the walls were more defined, yet interconnected by fibers (Figure S6). A further increase of the HA content (2.5 and 5 wt %) resulted in coalescence of the main and lateral fibers and a more defined closed-wall structure characterized by a collection of aligned channels interconnected with their neighbors.

Figure 2 compiles the relationship among the starting composition, the ice front rate, and the resultant scaffold

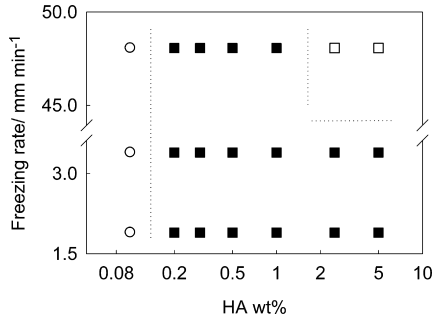

Figure 2. Morphology domains for bare HA–water systems: fibrilar (○), fibrilar-layered or open cells (■), and closed cells (□) as a function of freezing rate and HA concentration.

morphology. Structures formed by entangled fibers, denoted as open circles, were obtained with HA contents lower than 0.3 wt % and at almost every ice front rate.

This peculiar structure has been observed for other HA-based scaffolds[10,26,27] and could be related to the stiffened, random worm-like coil arrangement described for HA in diluted aqueous solutions.[28,29] The occurrence of fibers is partly due to the mutual electrostatic repulsion among carboxylate groups and mainly the existence of intramolecular hydrogen bonds that bridge adjacent monosaccharide units. This arrangement restricts rotation and flexion at glycosidic linkages that are in rapid exchange with water.[30−32] Because of the huge hydrodynamic volume, individual chains are brought into contact and begin to entangle with each other. This behavior was found even in solutions free of any added electrolyte.[33−35]

Closed-cell regime was observed for HA concentrations greater than 2.5 wt % and the fastest freezing rates, suggesting that parallel porous walls are more stable than random closed cells (Figure S7, S8). Between these extreme scenarios, a compromise situation resulted in a structure that could be described by parallel porous walls connected by fibers, as was observed for other biopolymers.[11,12,26,36−41]

Figure 3 shows the average pore diameter (longer and shorter) and the average wall thickness against the polymer concentration for scaffolds that exhibited well-defined pores; dimensions were measured from FESEM micrographs. In general, the greater the HA content, the larger the average pore diameter as well as the wall thickness. These results were substantially different from those previously obtained with other polymeric and ceramic biomaterials employed to produce tissue engineering scaffolds.[13,25] However, similar trends were observed in related systems for pore diameter and wall thickness.[42] The microstructural features observed with changes in HA concentration might also be ascribed to the ability of the system to form ice crystals that depends on the adsorption/desorption balance of such a solute on the surface of the ice crystal. Irreversible adsorption would completely abrogate ice-crystal growth, while full desorption would allow free crystal growth; solute adsorption and desorption on the ice surface are in dynamic equilibrium. For a particular solute, the effectiveness in inhibiting ice crystal growth is only related to the extent of coverage of the ice surface area by such a solute. Thus, to explain the changes on the morphology of HA scaffolds with the concentration it is important to take into account the changes in the conformation of HA (see comments above) and the interaction between HA and water molecules with concentration. Some authors showed that nonfreezing water or bound water can inhibit ice crystal formation depending on

dx.doi.org/10.1021/bm300814h | *Biomacromolecules* 2013, 14, 1–9

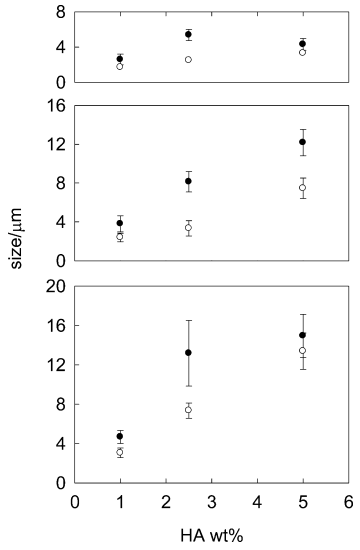

Figure 3. Wall thickness (upper panel), minor pore diameter (middle panel), and major pore diameter (lower panel) for samples frozen at 48 (●), and 3.6 (○) mm min^{-1}, as a function of the HA concentration.

HA; for semidiluted HA solutions, they attributed an antinucleation effect due to the existence of the HA network and its ability to inhibit formation and growth of ice nuclei. On the other hand, they showed a nucleation-enhancing effect for concentrations greater than 2 wt % and proposed that this effect may arise from the formation of HA aggregates, that could serve as nucleation aids.[43−45]

Effect of pH and Thermally Driven Prehydrolysis. Beyond the physical variables employed to tune the structure of native HA matrices, additional chemically based strategies could be applied to modify its behavior during ISISA, in order to manipulate the HA structure at a molecular level and consequently expand the structure formation possibilities.[46,47] In general terms, the segregation process developed by the polymer chains would be controlled to a great extent by the diffusion coefficient. This parameter will be affected by the intrinsic molecular weight of the individual chains and/or the degree of specific interaction between those polymer chains that govern the way in which they self-assemble into higher clusters. Thus, the process can be altered whenever HA undergoes irreversible hydrolysis, typically at a pH value below 4 and above 11. Between these extreme pH conditions, chain scission is negligible, this phenomenon being dependent on the temperature.[48] Under acid conditions, the cleavage of polymer chains (generally attributed to glycosidic linkages) leads to disengagement of chains and to disintegration of the polymer network.[49−51] Conversely, it was proposed that the disassembly of chain−chain interactions due to alkalinization (or heating) relies on the disruption of hydrogen-bonding and hydrophobic interactions among antiparallel HA chains.[52] In this context, even at neutral pH, native HA macromolecules dissolved in water could undergo significant hydrolysis at 60 °C or higher temperatures.[43,52,53] Concerning the factors that govern the interaction and association of HA molecules in solution, variables such as pH and ionic strength could also affect the

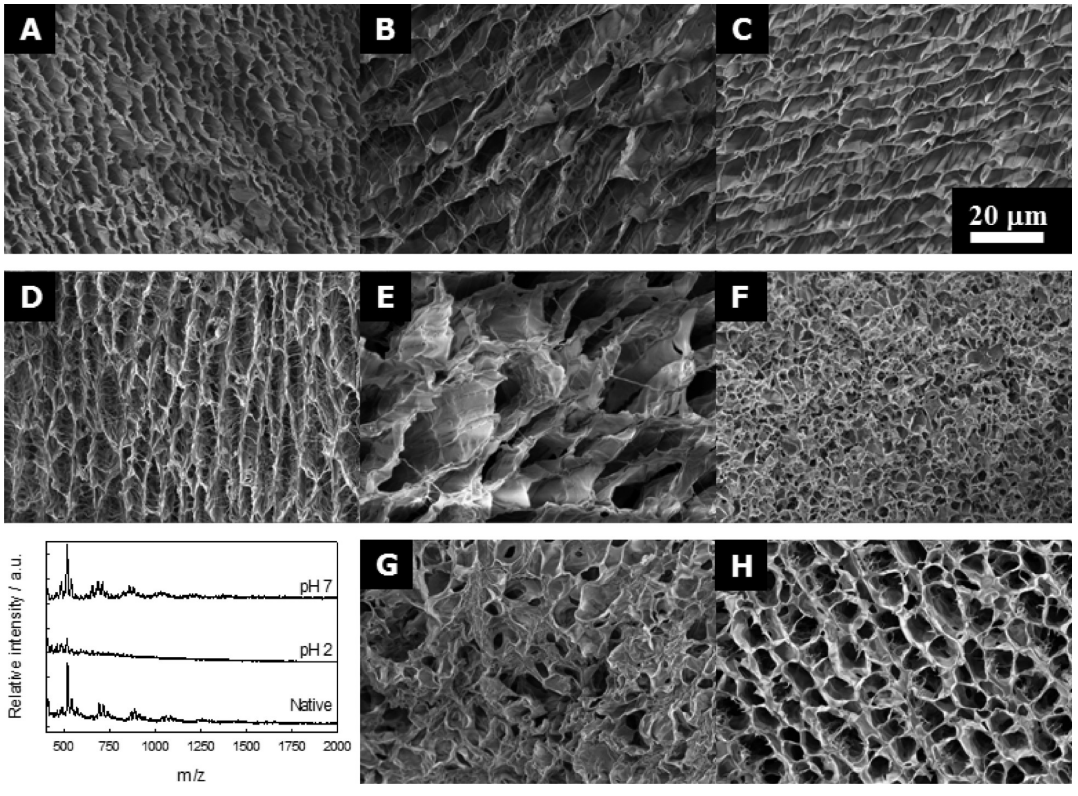

Figure 4. Representative morphology of samples frozen at a freezing rate of 3.6 mm min^{-1}, observed as a function of pH and thermal hydrolysis for 24 h at 60 °C. Thermally hydrolyzed samples are denoted with the suffix T. Otherwise, samples were hydrolyzed for 24 h at room temperature: H-2.5 native (A), pH 7 (B), pH 7-T (C), H-5.0 native (D), pH 7 (E), pH 7-T (F), pH 2 (G), pH 2-T (H). Scale bar depicted for sample A is valid for all images. Inset bottom left: MALDI-TOF spectra of HA in native conditions and after thermal hydrolysis at pH 7 and 2.

dx.doi.org/10.1021/bm300814h | *Biomacromolecules* 2013, 14, 1−9

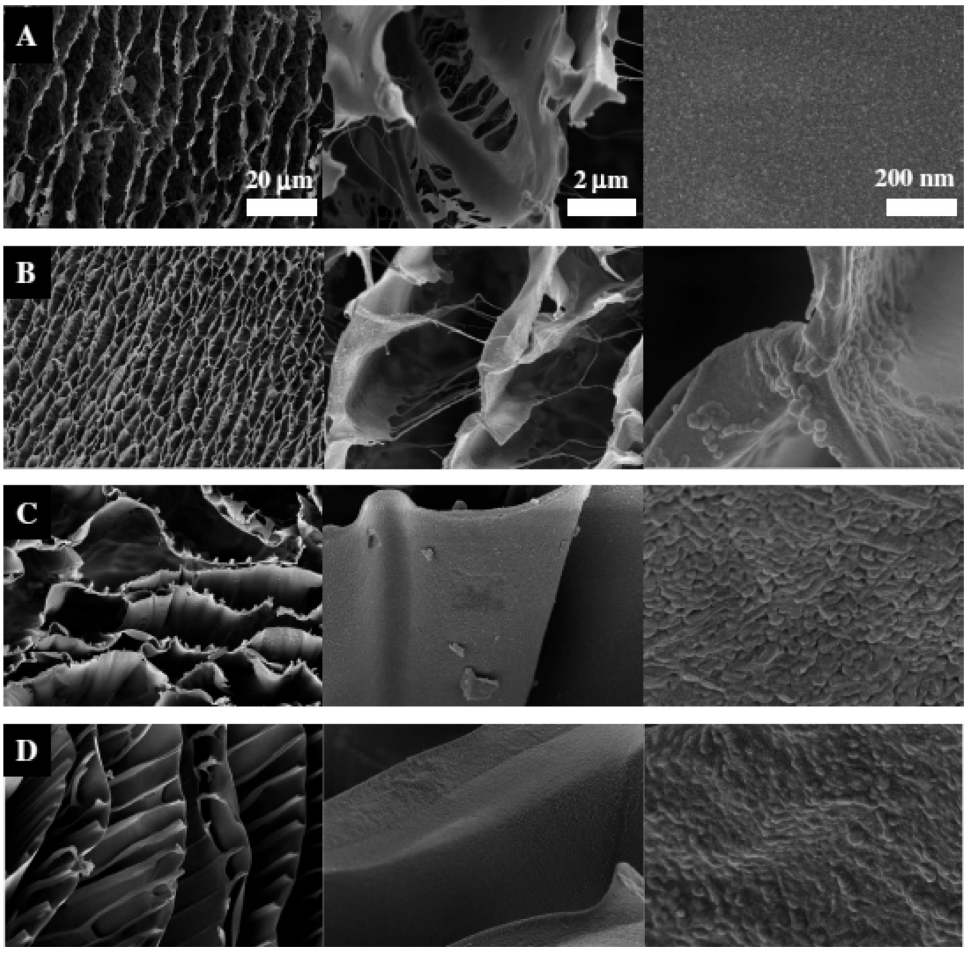

Figure 5. FESEM images of H-2.5 frozen at 48 mm min^{-1} (A) and H-2.5-G frozen at 48 (B), 3.6 (C), and 1.8 (D) mm min^{-1}. Scale bars depicted in A are valid for all images on the same row. The G concentration in the precursor solution is 2.0%.

rheological properties of HA aqueous solutions and result in significant changes at a molecular level that alter the structure formation process.[28,35,50,51]

In order to exemplify to what extent the aforementioned variables affected the HA scaffold microstructure, 2.5 and 5 wt % HA samples frozen at a freezing rate of 3.6 mm min^{-1} were exposed to (i) different pH conditions at room temperature and (ii) a mild thermal hydrolysis at 60 °C, for 24 h (Figure 4). Samples treated with 0.9% NaCl (with physiological ionic strength) as supporting electrolyte were included as controls.[28] The sample showed a cell-like microstructure connected by fibers (Figure 4A,D); when HA solutions in 0.9% NaCl were hydrolyzed at room temperature, both microstructure and pore size showed the same trend (data not shown). At pH 2, the scaffold structure was cell-like, connected by fibers with very variable pore size (Figure 4G,H). Regardless of the temperature, at pH 7, structures were similar to the native one but with larger pore size, this effect being only attributable to the increasing ionic strength. At pH 12, structures were also cell-like, though without connecting fibers (Figure S9). Furthermore, the wall thickness increased with the pH. In accordance with our results, pore and wall size of native and pH 7 2.5 wt % HA samples were very similar. The small difference could be attributed to the increment of the ionic strength (0.15 M NaCl in 2.5 wt % at pH 7) and its correlation with a different polymer conformation.[51,54]

During ISISA, the formation of small or large ice crystals is also related to the features of the solute (e.g., molecular size). In addition, the growth of an ice crystal depends on the surface interaction between the growing crystal and the particular solute. As a consequence, the differences observed in the microstructure and the smaller pore size under acid and alkaline conditions could be assigned to the disaggregation produced by the hydrolysis at both extreme pH values (2 and 12). In other words, hydrolysis increased the fraction of smaller polymer chains that could entrap more ice crystals, giving place to more pores of smaller size. Following a similar trend, the pore size of samples exposed to heating was smaller. These findings were in accordance with previous studies that showed changes in HA molecular weight for different pH and temperatures as a function of time.[51,52,55] Exposure to acid medium combined with thermal treatment resulted in a decrease of the HA molecular weight,[43,52] while at neutral pH, the hydrolysis was negligible.[51] MALDI assays confirmed the HA molecular weight drop after acid and basic thermal hydrolysis (60 °C, 24 h), while a sample aged at neutral condition remained almost indistinguishable from native HA (Figure 4, inset; Figure S10).

Effect of G on the Scaffold Microstructure. Once the influence of the main preparative variables on the microstructure of HA scaffolds was established, we assessed the effect of G incorporation. In this framework, representative samples of G-free H-1.0 and H-2.5 and their G-loaded counterparts H-1.0-G and H-2.5-G were thoroughly characterized; drug-loaded

samples containing 2.0% of G in the precursor solution. A 2.0 wt % gentamicin sulfate solution was submitted to ISISA, revealing a globular and irregular texture with no signs of crystallization (Figure S11). Recent works also reported on this behavior for this drug.[57] FESEM images of H-2.5-G reveal that the resulting structures were essentially similar to G-free HA-2.5, exhibiting walls interconnected by fibrillar bridges (Figure 5). The H-2.5-G sample frozen at lower rates changed to a lamellar regime, with an almost unaltered wall thickness (Figure 5). However, for all HA-2.5-G samples, irrespective of the freezing rate, a detailed inspection of the wall surface denoted the presence of occluded globules of size 30 ± 10 nm embedded in the otherwise smooth surface of the bare HA structure. H-1.0 samples displayed a similar trend though the presence of G clusters on the surface of the scaffold was more noticeable (Figure S12). As opposed to other related biopolymer−drug binary systems, PXRD analysis confirmed the absence of segregation of large G crystals.[56,57] While the freezing speed yet exerted a strong influence on the HA scaffold structure, the size of the observed globules remained almost unaltered.

Aiming to gain a deeper insight into the HA/G interaction, representative samples and controls were analyzed by DSC (Figures S13−15). G-free HA-2.5 frozen at 48 mm min^{-1} showed the presence of a broad endothermic peak around 100 °C, commonly associated with the loss of water molecules that remained within the scaffold after the lyophilization; two overlapped exothermic peaks centered around 235 and 245 °C probably corresponded to irreversible decomposition phenomena.[23,58−60] HA-2.5 frozen at slower rates of 1.8 and 3.6 mm min^{-1} revealed an additional endothermic peak centered at 210 °C that could be ascribed to the rearrangement of HA chains before decomposition due to a more organized intramolecular arrangement. The smaller heat involved during the first transition suggested a weaker interaction with water molecules. Below 200 °C, the thermal behavior of pure G (drug control) was similar to that HA, except for the appearance of certain well-defined satellite endothermic peaks, centered at 60 and 100 °C (and mounted over the broad peak) that could be also associated with water desorption (data not shown). Massive decomposition was evidenced by a single exotherm centered at 235 °C. In contrast with the separate components, H-2.5-G samples evidenced dramatic changes that depended on the ISISA conditions. The faster the freezing rate, the more noticeable the presence of a sharp endothermic peak centered at 225 °C. This phenomenon suggested the melting of an intimate HA/G blend, before massive decomposition. Conversely, slowest freezing rates resulted in decomposition patterns that were similar to those of HA/G physical mixtures, suggesting the segregation of G-rich amorphous domains within the scaffold (Figure S15).

Swelling and Gentamicin (G) Release/Permeation Kinetics. Since these scaffolds are envisaged for the prevention and treatment of skin wound infections and skin repair, a key property such as the swelling kinetics was evaluated for both bare and G-loaded HA scaffolds. Results, expressed as percentage of mass increase, evidenced very dissimilar behaviors that depended on the monolith composition and the freezing rate (Figure 6). Irrespective of the different saturation values, all the G-free samples showed a dramatic swelling during the first 15 min of the assay, reaching saturation in less than 1 h and remaining stable with no dissolution for 2 h. These data were in good agreement with recent reports.[23]

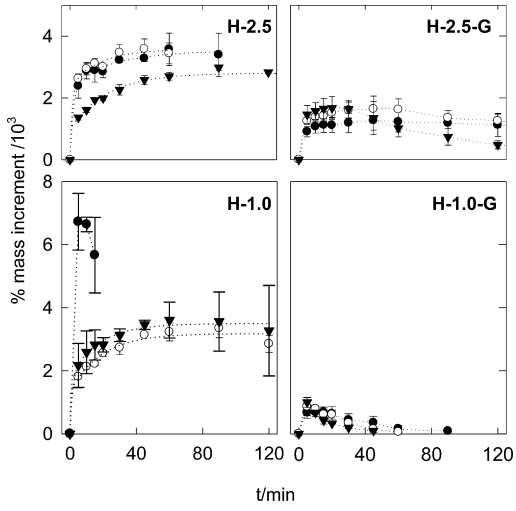

Figure 6. Swelling behavior of native HA control samples containing 2.5 and 1 wt % of HA (labeled as H-2.5 and H-1.0, respectively) and the HA samples loaded with extra content of G (labeled as H-2.5-G and H-1.0-G, respectively) frozen at 1.8 (▼), 3.6 (○), and 48 (●) mm min^{-1}.

However, H-1.0 frozen at the fastest rate (48 mm min^{-1}) exhibited an instant water uptake of approximately 70 times its dry weight, followed by massive dissolution after 20 min exposure. These results indicated that the open and disordered structure played a key role. Almost all of the remnant samples reached a similar maximum swelling, being able to incorporate around 35 times their dry mass in water. This value was slightly lower only in the case of H-2.5 frozen at minimum rate, even after 3 h, suggesting that the better structure formation characterized by denser walls resulted in a lower wettability, a less expandable scaffold, or a combination of both. Once G was added to the system, both H-2.5-G and H-1.0-G exhibited a much more moderate water uptake than their bare HA counterparts (Figure 6). This behavior was independent of the freezing conditions, suggesting that G makes the surface of HA scaffold more wettable and leads to a faster dissolution and massive mass loss before a greater swelling extent could be attained. This phenomenon was especially remarkable for H-1.0-G samples that dissolved in a matter of minutes (Figure 6).

The G release kinetics was assessed only in H-2.5-G samples; the extremely fast dissolution rate observed for H-1.0-G samples hindered a robust and reliable assessment of their release behavior. Release profiles are depicted in Figure 7. In general terms, samples frozen at 3.6 and 48 mm min^{-1} were

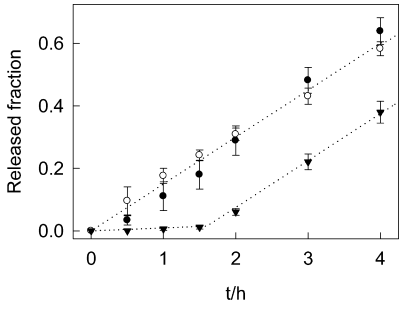

Figure 7. Cumulative release profile of H-2.5-G, frozen at 1.8 (▼), 3.6 (○), and 48 (●) mm min^{-1}.

dx.doi.org/10.1021/bm300814h | Biomacromolecules 2013, 14, 1−9

almost indistinguishable and they fitted the Korsmeyer-Peppas model[61] expressed by eq 1

$$M_t/M_\infty = k.\ t^n \quad (1)$$

where M_t is the amount of drug permeated at time t; M_∞, the amount of drug at infinite time; M_t/M_∞, the fraction of permeated drug (typically obtained from M_t/M_∞ values lower than 0.6); k, a kinetic constant, and n, a release exponent that depends on the sample geometry and the hydration behavior (Table S1). However, in certain matrices the release at the early stages is strongly governed by the hydration kinetics, resulting in an expression (eq 2) that considers the lag time associated with swelling and plasticization of the system[62−64]

$$M_t/M_\infty = k.\ (t - t_{lag})^n \quad (2)$$

Samples frozen at 3.6 and 48 mm min^{-1} could be described in terms of eq 1, with a k value of 0.15 h^{-1}, assuming a film-like geometry (n = 1). Results indicated a release process controlled by Fickian diffusion overlapped with matrix relaxation from a starting rigid (glass) state to a flexible swelled (rubber) one, also called transport case II. In this case, water molecules penetrate the matrix and play the role of plasticizer, since it decreases the glass transition temperature (T_g) of the material; once T_g reaches the appropriate value to enable the release of the drug, polymer chains undergo a marked volume expansion, resulting in a higher mobility that is in accordance with the observed swelling profiles. Despite the common structural and swelling features, samples frozen at 1.8 mm min^{-1} could not be properly described with the simple expression of eq 1 because the drug release was noticeable only after 2 h. However, after this lag period, it behaved almost identically to the others. Then, it could be described in terms of eq 2, with a k value of 0.15 h^{-1}, a lag period of 1.6 h, and assuming a film-like geometry (n = 1). The observed delay could be related to the segregation of G-rich domains, as suggested by DSC data. Bare HA control samples cannot dissolve before 2 h, suggesting that an external surface enriched in HA is responsible for the delayed dissolution observed with respect to the intimate mixture observed in the other samples where G was likely dispersed at the molecular level.

CONCLUSIONS

The ISISA process allowed the preparation of HA matrices with a huge variety of microarchitectures; depending on the desired application, their behavior in water could range from highly soluble fibers to more stable and swellable hydrogels. The native HA could be easily altered in terms of both its inter- and intramolecular interactions as well as its inherent molecular weight by changes in the pH and eventually, thermally driven hydrolysis, affecting the resulting textures. It was shown that samples exhibiting similar textures achieved different degrees of interdispersion between HA and G, resulting in the occurrence of a lag time for release. In parallel, samples with certain structural differences behaved similarly in terms of release, since both reached a high degree of interdispersion between HA and G. Then, the latter factor, and not texture, seems to be the key parameter that governs the release performance. The method allowed the one-pot consolidation of G-loaded HA matrices with variable drug/matrix interdispersion degree at a molecular level, resulting in tunable release kinetics, as certain applications require.[65,66] It is worth stressing that, for certain biomedical applications, more mechanically stable systems that sustain the drug release over more prolonged times could be required. In this context, the combination of HA with other types of water-soluble natural or synthetic polymers for the production of hybrid scaffolds should be assessed.

ASSOCIATED CONTENT

Supporting Information

Additional FESEM images, DSC measurements, and MALDI profiles. This material is available free of charge via the Internet at http://pubs.acs.org.

AUTHOR INFORMATION

Corresponding Author

*E-mail: jobbag@qi.fcen.uba.ar. Phone/Fax: +54-11-4576-3341.

Notes

The authors declare no competing financial interest.

ACKNOWLEDGMENTS

This work was supported by the University of Buenos Aires (UBACyT X-003), by Agencia Nacional de Promoción Científica y Tecnológica (ANPCyT PICT 06-33973), and by National Science Research Council of Argentina (CONICET PIP 112-200801-02533269; PIP 0220, UBACyT W636). Y.M. acknowledges a postdoctoral fellowship of CONICET. D.C., A.S., and M.J. are staff research scientists of CONICET (Argentina).

REFERENCES

(1) Hollister, S. J. Porous scaffold design for tissue engineering. *Nat. Mater.* **2005**, *4* (7), 518−524.

(2) Jones, J. R.; Ehrenfried, L. M.; Hench, L. L. Optimising bioactive glass scaffolds for bone tissue engineering. *Biomaterials* **2006**, *27* (7), 964−973.

(3) Ohtsuki, C.; Kokubo, T.; Yamamuro, T. Mechanism of Apatite Formation on CaO-SiO2-P2O5 Glasses in a Simulated Body-Fluid. *J. Non-Cryst. Solids* **1992**, *143* (1), 84−92.

(4) Rezwan, K.; Chen, Q. Z.; Blaker, J. J.; Boccaccini, A. R. Biodegradable and bioactive porous polymer/inorganic composite scaffolds for bone tissue engineering. *Biomaterials* **2006**, *27* (18), 3413−3431.

(5) Kokubo, T.; Kim, H. M.; Kawashita, M. Novel bioactive materials with different mechanical properties. *Biomaterials* **2003**, *24* (13), 2161−2175.

(6) Gutiérrez, M. C.; Jobbágy, M.; Ferrer, M. L.; Del Monte, F. Enzymatic synthesis of amorphous calcium phosphate-chitosan nanocomposites and their processing into hierarchical structures. *Chem. Mater.* **2008**, *20* (1), 11−13.

(7) Burdick, J. A.; Prestwich, G. D. Hyaluronic Acid Hydrogels for Biomedical Applications. *Adv. Mater.* **2011**, *23* (12), H41−H56.

(8) Necas, J.; Bartosikova, L.; Brauner, P.; Kolar, J. Hyaluronic acid (hyaluronan): a review. *Veterinarni Medicina* **2008**, *53* (8), 397−411.

(9) Park, S. N.; Kim, J. K.; Suh, H. Evaluation of antibiotic-loaded collagen-hyaluronic acid matrix as a skin substitute. *Biomaterials* **2004**, *25* (17), 3689−3698.

(10) Tang, S.; Vickers, S. M.; Hsu, H. P.; Spector, M. Fabrication and characterization of porous hyaluronic acid-collagen composite scaffolds. *J. Biomed. Mater. Res., Part A* **2007**, *82* (2), 323−335.

(11) Lee, C. T.; Lee, Y. D. Preparation of porous biodegradable poly(lactide-co-glycolide)/hyaluronic acid blend scaffolds: Characterization, in vitro cells culture and degradation behaviors. *J. Mater. Sci.: Mater. Med.* **2006**, *17* (12), 1411−1420.

(12) Hong, S. R.; Chong, M. S.; Lee, S. B.; Lee, Y. M.; Song, K. W.; Park, M. H.; Hong, S. H. Biocompatibility and biodegradation of cross-linked gelatin/hyaluronic acid sponge in rat subcutaneous tissue. *J. Biomater. Sci., Polym. Ed.* **2004**, *15* (2), 201−214.

(13) Gutierrez, M. C.; Ferrer, M. L.; del Monte, F. Ice-templated materials: Sophisticated structures exhibiting enhanced functionalities obtained after unidirectional freezing and ice-segregation-induced self-assembly. *Chem. Mater.* **2008**, *20* (3), 634−648.
(14) Zhang, H.; Hussain, I.; Brust, M.; Butler, M. F.; Rannard, S. P.; Cooper, A. I. Aligned two- and three-dimensional structures by directional freezing of polymers and nanoparticles. *Nat. Mater.* **2005**, *4* (10), 787−793.
(15) Munch, E.; Launey, M. E.; Alsem, D. H.; Saiz, E.; Tomsia, A. P.; Ritchie, R. O. Tough, Bio-Inspired Hybrid Materials. *Science* **2008**, *322* (5907), 1516−1520.
(16) Minaberry, Y.; Jobbagy, M. Macroporous Bioglass Scaffolds Prepared by Coupling Sol-Gel with Freeze Drying. *Chem. Mater.* **2011**, *23* (9), 2327−2332.
(17) Mukai, S. R.; Nishihara, H.; Tamon, H. Morphology maps of ice-templated silica gels derived from silica hydrogels and hydrosols. *Microporous Mesoporous Mater.* **2008**, *116* (1−3), 166−170.
(18) Nishihara, H.; Iwamura, S.; Kyotani, T. Synthesis of silica-based porous monoliths with straight nanochannels using an ice-rod nanoarray as a template. *J. Mater. Chem.* **2008**, *18* (31), 3662−3670.
(19) Deville, S. Freeze-casting of porous ceramics: A review of current achievements and issues. *Adv. Eng. Mater.* **2008**, *10* (3), 155−169.
(20) Deville, S.; Maire, E.; Bernard-Granger, G.; Lasalle, A.; Bogner, A.; Gauthier, C.; Leloup, J.; Guizard, C. Metastable and unstable cellular solidification of colloidal suspensions. *Nat. Mater.* **2009**, *8* (12), 966−972.
(21) Deville, S.; Maire, E.; Lasalle, A.; Bogner, A.; Gauthier, C.; Leloup, J.; Guizard, C. In Situ X-Ray Radiography and Tomography Observations of the Solidification of Aqueous Alumina Particle Suspensions-Part I: Initial Instants. *J. Am. Ceram. Soc.* **2009**, *92* (11), 2489−2496.
(22) Khan, F.; Walsh, D.; Patil, A. J.; Perriman, A. W.; Mann, S. Self-organized structural hierarchy in mixed polysaccharide sponges. *Soft Matter* **2009**, *5* (16), 3081−3085.
(23) Collins, M. N.; Birkinshaw, C. Morphology of Cross linked Hyaluronic Acid Porous Hydrogels. *J. Appl. Polym. Sci.* **2011**, *120* (2), 1040−1049.
(24) Deville, S.; Saiz, E.; Tomsia, A. P. Ice-templated porous alumina structures. *Acta Mater.* **2007**, *55* (6), 1965−1974.
(25) Gutierrez, M. C.; Garcia-Carvajal, Z. Y.; Jobbagy, M.; Rubio, T.; Yuste, L.; Rojo, F.; Ferrer, M. L.; del Monte, F. Poly(vinyl alcohol) scaffolds with tailored morphologies for drug delivery and controlled release. *Adv. Funct. Mater.* **2007**, *17* (17), 3505−3513.
(26) Wang, T. W.; Spector, M. Development of hyaluronic acid-based scaffolds for brain tissue engineering. *Acta Biomater.* **2009**, *5* (7), 2371−2384.
(27) Park, S.-N.; Park, J.-C.; Kim, H. O.; Song, M. J.; Suh, H. Characterization of porous collagen/hyaluronic acid scaffold modified by 1-ethyl-3-(3-dimethylaminopropyl)carbodiimide cross-linking. *Biomaterials* **2002**, *23* (4), 1205−1212.
(28) Cowman, M. K.; Matsuoka, S. Experimental approaches to hyaluronan structure. *Carbohydr. Res.* **2005**, *340* (5), 791−809.
(29) Hayashi, K.; Tsutsumi, K.; Norisuye, T.; Teramoto, A. Electrostatic contributions to chain stiffness and excluded-volume effects in sodium hyaluronate solutions. *Polym. J.* **1996**, *28* (10), 922−928.
(30) Morris, E. R.; Rees, D. A.; Welsh, E. J. Conformation and dynamic interactions in hyaluronate solutions. *J. Mol. Biol.* **1980**, *138* (2), 383−400.
(31) Almond, A.; Sheehan, J. K.; Brass, A. Molecular dynamics simulations of the two disaccharides of hyaluronan in aqueous solution. *Glycobiology* **1997**, *7* (5), 597−604.
(32) Almond, A.; Brass, A.; Sheehan, J. K. Dynamic exchange between stabilized conformations predicted for hyaluronan tetrasaccharides: Comparison of molecular dynamics simulations with available NMR data. *Glycobiology* **1998**, *8* (10), 973−980.
(33) Furlan, S.; La Penna, G.; Perico, A.; Cesaro, A. Hyaluronan chain conformation and dynamics. *Carbohydr. Res.* **2005**, *340* (5), 959−970.
(34) Ghosh, S.; Li, X.; Reed, C. E.; Reed, W. F. Apparent persistence lengths and diffusion behavior of high molecular weight hyaluronate. *Biopolymers* **1990**, *30* (11−12), 1101−1112.
(35) Reed, C. E.; Li, X.; Reed, W. F. The Effects of Ph on Hyaluronate as Observed by Light-Scattering. *Biopolymers* **1989**, *28* (11), 1981−2000.
(36) Garcia-Fuentes, M.; Meinel, A. J.; Hilbe, M.; Meinel, L.; Merkle, H. P. Silk fibroin/hyaluronan scaffolds for human mesenchymal stem cell culture in tissue engineering. *Biomaterials* **2009**, *30* (28), 5068−5076.
(37) Qian, L.; Ahmed, A.; Foster, A.; Rannard, S. P.; Cooper, A. I.; Zhang, H. Systematic tuning of pore morphologies and pore volumes in macroporous materials by freezing. *J. Mater. Chem.* **2009**, *19* (29), 5212−5219.
(38) Tan, H.; Ramirez, C. M.; Miljkovic, N.; Li, H.; Rubin, J. P.; Marra, K. G. Thermosensitive injectable hyaluronic acid hydrogel for adipose tissue engineering. *Biomaterials* **2009**, *30* (36), 6844−6853.
(39) Liu, H.; Yin, Y.; Yao, K. Construction of chitosan-gelatin-hyaluronic acid artificial skin in vitro. *J. Biomater. Appl.* **2007**, *21* (4), 413−430.
(40) Barbucci, R.; Consumi, M.; Magnani, A. Dependence of water uptake and morphology of hyaluronan- and alginate-based hydrogels on pH and degree of crosslinking. *Macromol. Chem. Phys.* **2002**, *203* (10−11), 1292−1300.
(41) Mao, J. S.; Liu, H. F.; Yin, Y. J.; Yao, K. D. The properties of chitosan-gelatin membranes and scaffolds modified with hyaluronic acid by different methods. *Biomaterials* **2003**, *24* (9), 1621−1629.
(42) Kim, J. W.; Taki, K.; Nagamine, S.; Ohshima, M. Preparation of poly(L-lactic acid) honeycomb monolith structure by unidirectional freezing and freeze-drying. *Chem. Eng. Sci.* **2008**, *63* (15), 3858−3863.
(43) Matteini, P.; Dei, L.; Carretti, E.; Volpi, N.; Goti, A.; Pini, R. Structural behavior of highly concentrated hyaluronan. *Biomacromolecules* **2009**, *10* (6), 1516−1522.
(44) Liu, J.; Cowman, M. K. Thermal analysis of semi-dilute hyaluronan solutions. *J. Therm. Anal. Calorim.* **2000**, *59* (1−2), 547−557.
(45) Takahashi, M.; Hatakeyama, T.; Hatakeyama, H. Phenomenological theory describing the behaviour of non-freezing water in structure formation process of polysaccharide aqueous solutions. *Carbohydr. Polym.* **2000**, *41* (1), 91−95.
(46) Horkay, F.; Basser, P. J.; Londono, D. J.; Hecht, A. M.; Geissler, E. Ions in hyaluronic acid solutions. *J. Chem. Phys.* **2009**, *131*, (18).
(47) TØmmeraas, K.; Melander, C. Kinetics of hyaluronan hydrolysis in acidic solution at various pH values. *Biomacromolecules* **2008**, *9* (6), 1535−1540.
(48) Maleki, A.; Kjoniksen, A. L.; Nystrom, B. Effect of pH on the Behavior of Hyaluronic Acid in Dilute and Semidilute Aqueous Solutions. *Macromol. Symp.* **2008**, *274*, 131−140.
(49) Furlan, S.; La Penna, G.; Perico, A.; Cesáro, A. Hyaluronan chain conformation and dynamics. *Carbohydr. Res.* **2005**, *340* (5), 959−970.
(50) Gatej, L.; Popa, M.; Rinaudo, M. Role of the pH on hyaluronan behavior in aqueous solution. *Biomacromolecules* **2005**, *6* (1), 61−67.
(51) Tommeraas, K.; Melander, C. Kinetics of hyaluronan hydrolysis in acidic solution at various pH values. *Biomacromolecules* **2008**, *9* (6), 1535−1540.
(52) Scott, J. E.; Heatley, F. Biological properties of hyaluronan in aqueous solution are controlled and sequestered by reversible tertiary structures, defined by NMR spectroscopy. *Biomacromolecules* **2002**, *3* (3), 547−553.
(53) Stern, R.; Kogan, G.; Jedrzejas, M. J.; Soltes, L. The many ways to cleave hyaluronan. *Biotechnol. Adv.* **2007**, *25*, 537−557.
(54) Buhler, E.; Boue, F. Chain persistence length and structure in hyaluronan solutions: Ionic strength dependence for a model semirigid polyelectrolyte. *Macromolecules* **2004**, *37* (4), 1600−1610.

(55) Drímalová, E.; Velebná, V.; Sasinková, V.; Hromádková, Z.; Ebringerová, A. Degradation of hyaluronan by ultrasonication in comparison to microwave and conventional heating. *Carbohydr. Polym.* **2005**, *61* (4), 420−426.
(56) Aranaz, I.; Gutiérrez, M. C.; Yuste, L.; Rojo, F.; Ferrer, M. L.; Del Monte, F. Controlled formation of the anhydrous polymorph of ciprofloxacin crystals embedded within chitosan scaffolds: Study of the kinetic release dependence on crystal size. *J. Mater. Chem.* **2009**, *19* (11), 1576−1582.
(57) Ouedraogo, M.; Semde, R.; Some, I. T.; Ouedraogo, R. T.; Guissou, I. P.; Henschel, V.; Dubois, J.; Amighi, K.; Evrard, B. Monoolein-water liquid crystalline gels of gentamicin as bioresorbable implants for the local treatment of chronic osteomyelitis: In vitro characterization. *Drug Dev. Ind. Pharm.* **2008**, *34* (7), 753−760.
(58) Villetti, M. A.; Crespo, J. S.; Soldi, M. S.; Pires, A. T. N.; Borsali, R.; Soldi, V. Thermal degradation of natural polymers. *J. Therm. Anal. Calorim.* **2002**, *67* (2), 295−303.
(59) Collins, M. N.; Birkinshaw, C. Physical properties of crosslinked hyaluronic acid hydrogels. *J. Mater. Sci.: Mater. Med.* **2008**, *19* (11), 3335−3343.
(60) Benesova, K.; Pekar, M.; Lapcik, L.; Kucerik, J. Stability evaluation of n-alkyl hyaluronic acid derivates by DSC and TG measurement. *J. Therm. Anal. Calorim.* **2006**, *83* (2), 341−348.
(61) Korsmeyer, R. W.; Gurny, R.; Doelker, E.; Buri, P.; Peppas, N. A. Mechanisms of Solute Release from Porous Hydrophilic Polymers. *Int. J. Pharm.* **1983**, *15* (1), 25−35.
(62) González, B.; Colilla, M.; Vallet-Regí, M. Time-delayed release of bioencapsulates: A novel controlled delivery concept for bone implant technologies. *Chem. Mater.* **2008**, *20* (15), 4826−4834.
(63) Kim, H.; Fassihi, R. Application of binary polymer system in drug release rate modulation 0.2. Influence of formulation variables and hydrodynamic conditions on release kinetics. *J. Pharm. Sci.* **1997**, *86* (3), 323−328.
(64) Pillay, V.; Fassihi, R. In vitro release modulation from crosslinked pellets for site-specific drug delivery to the gastrointestinal tract - I. Comparison of pH-responsive drug release and associated kinetics. *J. Controlled Release* **1999**, *59* (2), 229−242.
(65) Kelly, R. M.; Meyer, J. D.; Matsuura, J. E.; Shefter, E.; Hart, M. J.; Malone, D. J.; Manning, M. C. In vitro release kinetics of gentamycin from a sodium hyaluronate gel delivery system suitable for the treatment of peripheral vestibular disease. *Drug Dev. Ind. Pharm.* **1999**, *25* (1), 15−20.
(66) Heijink, A.; Yaszemski, M. J.; Patel, R.; Rouse, M. S.; Lewallen, D. G.; Hanssen, A. D. Local antibiotic delivery with OsteoSet, DBX, and Collagraft. *Clin. Orthop. Relat. Res.* **2006**, *451*, 29−33.